

Article

Diagenetic Evolution of Upper Cretaceous Kawagarh Carbonates from Attock Hazara Fold and Thrust Belt, Pakistan

Saif Ur Rehman ^{1,*}, Muhammad Jawad Munawar ¹, Mumtaz Muhammad Shah ², Naveed Ahsan ¹,
Muhammad Kashif ³, Hammad Tariq Janjuhah ^{4,*}, Vasiliki Lianou ⁵ and George Kontakiotis ⁵

¹ Institute of Geology, University of the Punjab, Lahore 54590, Pakistan; jawad.geo@pu.edu.pk (M.J.M.); naveedahsan.geol@gmail.com (N.A.)

² Department of Earth Sciences, Quaid-e-Azam University, Islamabad 44000, Pakistan; mshah@qau.edu.pk

³ Department of Earth Sciences, University of Sargodha, Sargodha 40100, Pakistan; kashifyaqub@yahoo.com

⁴ Department of Geology, Shaheed Benazir Bhutto University, Sheringal 18050, Pakistan

⁵ Department of Historical Geology-Paleontology, Faculty of Geology and Geoenvironment, School of Earth Sciences, National and Kapodistrian University of Athens, 15784 Athens, Greece; vlianou@geol.uoa.gr (V.L.); gkontak@geol.uoa.gr (G.K.)

* Correspondence: saif.geo@pu.edu.pk (S.U.R.); hammad@sbbu.edu.pk (H.T.J.)

Abstract: A recent hydrocarbons discovery in 2021 in the Kawagarh Formation has brought attention to the significance of sedimentology and specifically diagenesis for understanding and characterizing the reservoir properties. The diagenetic history and multiscale processes that contributed to diagenesis were vaguely known. This study aimed to reconstruct various diagenetic phases, paragenetic sequences, and the interrelationship of these phases in the Kawagarh Formation. The diagenetic processes were identified and characterized through an integrated methodology utilizing the outcrop, petrographic, and geochemical analyses. Early calcite cementation was found to occur in the early stages of marine burial diagenesis involving pore fluid originating from the dissolution of aragonite in interlayer marl/mudstone beds and reprecipitating as microspar in adjacent limestone beds. The absence of mechanical compaction in wackstone and mudstone facies and the presence of late compaction in lithified packstones clearly imply that early calcite cementation occurred prior to compaction. Dolomitization with stylolites coupled with significant negative oxygen ($\delta^{18}\text{O}$) isotope values implies a fault-related hydrothermal dolomitization model. Uplift introduced the fractures and low Mg fresh fluids to the system which caused calcitisation in shallow burial settings. The depleted $\delta^{13}\text{C}$ and negative $\delta^{18}\text{O}$ values indicate the mixing of surface-derived waters with hot burial fluids during the calcitization. This study offers valuable insights into several aspects related to the formation and the basin itself, including burial depths, fluid influx, and geochemical gradients. It also sheds light on the evolution of reservoir properties such as porosity and permeability in dolomitization fronts. Such insights can be used to gain a deeper understanding about the burial history, basin evaluation, and reservoir characterization for hydrocarbon exploration.

Keywords: Kawagarh Formation; cretaceous; carbonate diagenesis; shallow marine depositional environment; early calcite cementation; dolomitization; reservoir characterization



Citation: Rehman, S.U.; Munawar, M.J.; Shah, M.M.; Ahsan, N.; Kashif, M.; Janjuhah, H.T.; Lianou, V.; Kontakiotis, G. Diagenetic Evolution of Upper Cretaceous Kawagarh Carbonates from Attock Hazara Fold and Thrust Belt, Pakistan. *Minerals* **2023**, *13*, 1438. <https://doi.org/10.3390/min13111438>

Academic Editors: Michael S. Zhdanov and José Javier Alvaro

Received: 1 September 2023

Revised: 23 October 2023

Accepted: 7 November 2023

Published: 13 November 2023



Copyright: © 2023 by the authors. Licensee MDPI, Basel, Switzerland. This article is an open access article distributed under the terms and conditions of the Creative Commons Attribution (CC BY) license (<https://creativecommons.org/licenses/by/4.0/>).

1. Introduction

Shallow water carbonates settings are sites where marine life flourishes; thus, they preserve and present excellent depositional and diagenetic records in oceanic environments [1]. Despite the simple mineralogy, carbonate rock poses extremely complex fabric and pore systems developed under composite diagenetic process [2]. These diagenetic processes are typically governed by the pore fluids which can significantly alter original depositional fabric and pore systems of the rock by dissolution, cementation, or mineral replacement. The chemical composition of pore fluids, the rate of fluid flux, and the temperature and pressure conditions under which rock-water interactions occur regulate the diagenetic

processes manipulating texture and porosity of carbonates [2–5]. Such processes mainly involve dissolution of extant mineral phases and/or precipitation of new mineral phases. Globally, reservoirs characterization has significantly stressed upon the diagenetic studies and porosity evolution in carbonate rocks [2,6–8]. Information such as primary rock fabric, porosity types, and timing of porosity development plays a critical role in geological reservoir models. These models are very important for the prediction of the distribution of favorable reservoir rock during the hydrocarbon migration [9].

There are three principal carbonate diagenetic environments (meteoric, marine, and burial) within which porosity development, evolution, and their distribution on the earth's surface or in the subsurface can be discussed [4,10–13]. The marine and meteoric environments commonly associated with near surface and surface environments are also called eogenetic and telogenetic zones [14]. The marine environments are the main source of carbonate deposition where the diagenesis is predominantly influenced by the supersaturated marine pore fluids. Ideal conditions are present in marine environments for the precipitation of calcite cement during the fluid percolation through the pore system [12,14,15]. The precipitation of new mineral phase and/or replacement of existing mineral phase by enriched fluids can bring unprecedented changes and can produce highly complex carbonate fabric and pore systems. The meteoric diagenetic environment is generally associated with the subaerial shallow marine carbonate depositional sequence [12,16]. The meteoric environments are represented by the zone of dilute waters which are moving at a strong rate from the vadose zone to the phreatic zone. The vadose zone commonly constitutes under-saturated states of carbonate mineral species due to the presence of CO₂ in meteoric water [10]. The dissolution of CaCO₃ is more active in the vadose zone and it produces a more depleted zone of CaCO₃ which leads to the formation of vugs and cavernous structures in limestone deposits. Among the subsurface conditions, burial diagenesis is the most significant that is encountered upon the deep burial of sedimentary deposits within the earth. It is active beyond near surface environments and marks the mesogenetic porosity zone [14]. The major diagenetic controlling agent in burial zone environments is the pressure, temperature, and formation water [12,17,18].

The diagenetic process naturally distributes the various mineral and pore phases spatially and temporally in such naturally complex patterns making it very difficult to understand and reconstruct the diagenetic phase. The Late Turonian Kawagarh Formation exhibits a unique library possessing spectacular marine, sedimentation, diagenetic, climatic, and tectonic records. Depositional environments and tectonic history have already been established by [19] and [20] in the Hazara and Kalachitta Range. However, diagenetic history and meso to micro scale processes drive multiscale diagenetic events, especially calcitization of lime mud in thick marls, strata bound dolomitization, and dedolomitization which were vaguely known. The first objective of this study is to find out and discuss the source and mechanism of early calcite cementation in the Kawagarh Formation, and particularly in its marls. The second objective is to investigate the stylolite and its relationship with dolomitization. This work is accomplished by utilizing a highly integrated diagenetic workflow based on a multiproxy geochemical approach. Each carbonate diagenetic phase is recognized and characterized through geochemical analyses: optical petrography, atomic absorption spectroscopy (AAS), and carbon and oxygen isotope. The present study provides invaluable context for the reconstruction of the history of the shallow ramp carbonates of the Kawagarh Formation and can serve as a reference for studying and documenting equivalent carbonate systems.

2. Geological Setting

Attock Hazara Fold and Thrust Belt (AHFTB), which is itself part of the Northwest Lesser Himalayas, presents a narrow EW trending strip comprised of thick sedimentary package with low grade metamorphic rocks along the hanging wall of the Nathiagali Thrust (NGT) in Northern Pakistan [21]. Geologically, it is surrounded by the Pan-

jal/Kherabad Fault in the north and bordered by the Main Boundary Fault (MBT) in the south (Figure 1) [19,22–24].

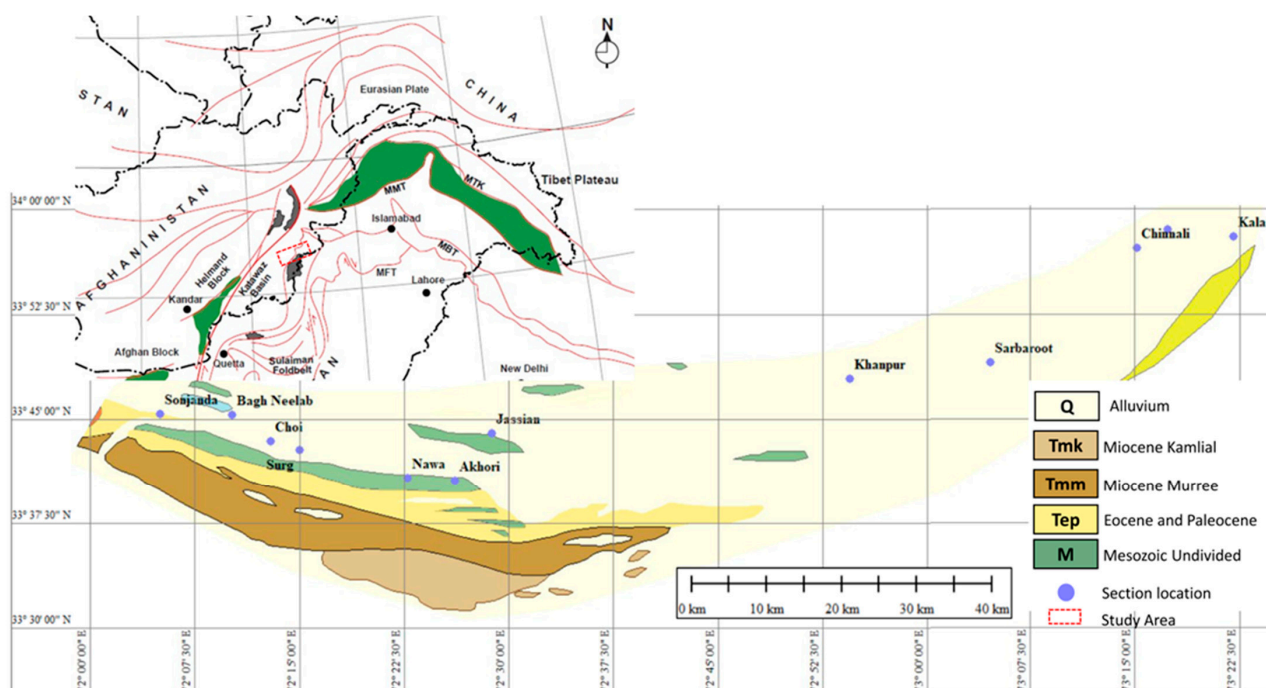


Figure 1. Geological map of the Hazar and Kala Chitta Basin showing the location of the studied sections.

Northern Pakistan is comprised of three convergence tectonic elements: the Indian Plate, the Kohistan-Ladakh Arc (KLA), and the Asian Plate from south to north [23,25–30]. This collision led to the development of the Himalaya Mountain range along the northern margin of the Indian Plate. The movement of the Indian Plate northwards caused older rocks to be thrust over younger strata, resulting in the formation of small fault-bounded blocks including the Trans Himalaya, Higher Himalaya, Lesser Himalaya, and Sub-Himalaya [31–33]. In the western Himalayan Basin (HB), the Lesser Himalayas of Pakistan are bounded by the Hissartang Fault in the north and the Indus River in the west, constituting the southernmost extension of the Himalayas [34]. The sedimentary succession in the region, from Triassic to Miocene-Pliocene, is tightly folded and cut by numerous thrust faults [35]. The Jurassic sedimentation consists of the Datta Formation, Shinawari Formation, and Samana Suk Formation (Figure 2). The Cretaceous succession includes the Chichali Shale, Lumshiwal Formation, and Kawagarh Formation. The Chichali Shale contains belemnite and pyrite and was deposited in anoxic restricted environments when the Indian Plate was separating from Gondwana [36]. The Kawagarh Formation is mainly comprised of limestone and marl with subordinate dolomite [20,21,24,37,38] that was deposited over a carbonate ramp formed due to the subsidence created by the northward drift of the Indian Plate [39].

Paleomagnetic data, zircon dating, and fossils in volcanic sediments suggest Early Cretaceous rifting and volcanism because of separation and drifting of the microcontinent and the opening of a new basin (Neo Tethys) at the northern margin of India [40,41]. Conferring to the faunal content and ecological attributes, the Kawagarh Formation is deposited in Neo Tethys under shallow open marine and well oxygenated conditions, suggesting a ramp setting [19,20,38,42]. The deposition initiated with transgressive depositional cycle at the base, with inner-ramp microfacies overlying the lateritised top of the underlying Lumshiwal Formation and overlain by mid-ramp and outer ramp microfacies [20,24]. The lateritisation suggests shallow water conditions and intense weathering induced by regression after the deposition of the Lumshiwal Formation [24]. This regression also corresponds to the early Turonian global sea level fall of [43], which partially exposed the Lumshiwal Formation

sediments. The regression during the late Turonian was followed by a transgression characterized by minor sea level fluctuations until the end of the Cretaceous with a general deepening upward sequence. The deposition of the Kawagarh Formation ended with the uplift of carbonate sediments during the Maastrichtian as shown in paleontological data and the presence of residual deposits of the K-Pc boundary at the top of the Kawagarh Formation [37,44]. The regional distribution of unconformity-related residual clays over the top of the Kawagarh Formation in the Attock Hazara Fold and Thrust Belt (AHFTB) and the complete absence of Upper Cretaceous sediments in the Sub-Himalayas in the south of the AHFTB suggest a regional event that uplifted these areas at the end of the Cretaceous [23,27,29,45–50]. The Indian Plate first collided with the KLA at the end of the Cretaceous or the Cretaceous-Paleocene boundary, terminating the depositional trend of the Kawagarh Formation due to the regional tectonic settings [23,27,29,45–50]. Generalized stratigraphic sequences of this study area are provided in Figure 2.

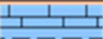
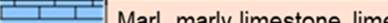
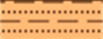
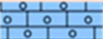
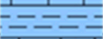
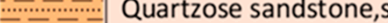
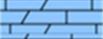
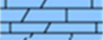
Age		Formation	Lithology
Cenozoic	Neogene	Miocene-Pliocene	Murree Formation  Sandstone & clays/shale With minor siltstone & Claystone
		Paleogene	Eocene
	Kohat Formation  Limestone & shale		
	Kuldana Formation  Shales, limestone & sandstone		
	Chorgali Formation  Limestone & shale		
	Margala Formation  Nodular limestone & marl		
	Paleocene		Patala Formation  Shales, limestone & sandstone
	Lockhart Limestone  Nodular limestone		
	Hangu Formation  Ferruginous Sandstone		
	Unconformity 		
Mesozoic	Cretaceous	Kawagarh Formation  Marl, marly limestone, limestone dolostone	
		Lumshiwai Formation  Sandstone & shale	
		Chichali Formation  Shale, minor sandstone	
		Disconformity 	
	Jurassic	Samana Suk Formation  Oolitic limestone	
		Shinawri Formation  Limestone, marl/shale	
		Datta Formation  Quartzose sandstone, shale	
		Unconformity 	
		Triassic	Kingriali Formation  Dolomite, Dolomitic limestone
	Chak Jabbri Limestone  Limestone		
	Mianwali Formation  Limestone, sandstone & shale		

Figure 2. Generalized stratigraphy and formation lithology of the Hazara and Kala Chitta Basin.

The Kawagarh Formation is mainly composed of grey to light grey limestone. The limestone is generally fine grained, thin to thick bedded, and occasionally very thick bedded. It is dolomitic at places and shows a sandy texture at the basal part. Dolomite is yellowish brown to rusty brown and pale yellow and at some places exhibits a sandy texture.

3. Materials and Methods

In the current study, we employed an integrated petrographic and geochemical approach to unravel the complex diagenetic history of the Cretaceous Kawagarh Formation in the Hazara and Kalachitta regions. Field observations and thin section microscopy were integrated to delineate the spatial and temporal diagenetic framework. Element chemistry (major, minor) and stable carbon and oxygen isotopes ($\delta^{13}\text{C}$, $\delta^{18}\text{O}$) were utilized to delineate processes which governed these diagenetic changes. A total of 256 samples from limestone, dolomite, and marl were analyzed to determine major (Ca, Mg) elements and trace elements (Fe, Sr, Mn, Na) chemistry. A same number of samples were used to determine bulk rock $\delta^{13}\text{C}$ and $\delta^{18}\text{O}$ isotope values.

3.1. Fieldwork and Sampling

We investigated twelve sections of the Cretaceous carbonate platform Kawagarh Formation, along an E-W transect from the Kalachitta and Hazara ranges of northern Pakistan (Figure 1). Four sections (Chinali, Kalas, Khanpur, Sarbaroot) from the Hazara Basin and seven sections (Akhori, Nawa, Sugdara, Bagh Neelab, Sojhanda Dam, Surg, and Jassian) from the Kalachitta ranges were studied. Microfacies and depositional environments of the Kalachitta sections have already been reported by [20].

Bed to bed sampling was carried out for limestone and dolomite while the marl samples were collected from embedded horizons between limestone or dolomite beds. The sections were measured considering that each rock unit should have complete exposure and maximum features with assured lateral extension and minimum deformation, while top and bottom should be well preserved, and deformation should be removed in case of faulting or folding. Detailed graphical sedimentary logs of the stratigraphic sections were constructed along with the recording of all necessary information including color, lithology, fossil content, and sedimentary structures.

3.2. Thin Section Microscopy

The samples were sliced perpendicular to the bedding plane with a diamond cutter to prepare the rock chips. These chips were ground to flatten the surface and polished with 100 μm particle sized carborundum abrasive powder. The polished chips were mounted on glass slides with a mixture of epoxy resin and hardener and ground on the other side to attain about 30 μm thickness. After that, the rock was polished with corundum powder (up to 0.8 μm particle size) to remove the residual surface abrasion and to maximize the textural resolution. Thin sections were stained in a solution of Alizarian Red S and Potassium ferricyanide solution for the differentiation of calcite from dolomite and to distinguish the ferron or non-ferron character of calcite [51,52]. Thin sections were examined under a polarizing microscope to record the microscopic data to establish paragenetic sequence, based on the superposition, crosscutting relationship, or overlap of diagenetic features. Field observations were also integrated with the thin sections study.

3.3. Major and Trace Element Stable Isotope Geochemistry

Samples were analyzed on an Atomic Absorption Spectrometer (AAS, AA 6300, Shimadzo) at High Tech Laboratory, University of Sargodha, Sargodha to measure the major (Ca, Mg) and trace elements (Fe, Sr, Mn, Na) chemistry. Samples were prepared following the method of [53]. Selected rock samples were crushed into fine powder and the powder was placed in an oven for 12 h at 100 °C. One gram sample of dried powder was dissolved in 50 mL of solution of 1N HCl for two hours. The dissolved solution was filtered using filter papers. A 0.5% KCl solution was added to the aforesaid solution to avoid further

reactions. Next, 100X solutions were prepared by adding 100mL of deionized water for the determination of major elements (Ca and Mg). Dilutions were prepared to the detectable limits of AAS.

Carbon ($\delta^{13}\text{C}$) (and oxygen ($\delta^{18}\text{O}$) isotope ratios from bulk rocks were analyzed at the Nanjing Institute of Geology and Palaeontology, Nanjing, China. The samples were washed, cleaned, and powdered to 75 μm grain size. This powder was treated with phosphoric acid in an automated process. The $\delta^{13}\text{C}$ and $\delta^{18}\text{O}$ ratios of bulk rock were reported in standard delta permil (‰) notation relative to Vienna Pee Dee Belemnite (V-PDB) calibrated with the international standards NBS-18 ($\delta^{13}\text{C} = -5.01\text{‰}$ VPDB; $\delta^{18}\text{O}$ of -23.1‰ VPDB) and NBS-19 ($\delta^{13}\text{C}$ of $+1.95\text{‰}$ VPDB; $\delta^{18}\text{O}$ of -2.20‰ VPDB).

4. Results

4.1. Petrography

Through extensive examination and delicate observation, we have documented the intricate details of diagenetic processes and their consequential effects on the fabric and mineralogical composition of the Kawagarh Formation. The petrography section presents an in-depth mineralogical, text, and fabric analysis, providing valuable insights into the complex diagenetic history of the Formation. We have undertaken conventional thin section microscopic analysis to unravel and elucidate five major diagenetic events that have significantly influenced the Kawagarh Formation. The identified diagenetic events encompass early calcite cementation (ECC) and neomorphism, compaction, and replacive dolomitization (RD), as well as the placement of fracture calcite (FC) and calcitization. The details of the diagenetic processes and their resultant fabrics are discussed in the following sections.

4.1.1. Early Calcite Cementation (ECC)

ECC is a well-studied and evolving aspect of carbonate diagenesis. Substantial literature is available on the morphology, growth, distribution, and types of cements [11,54–62]. Substantial features of early calcite cement such as microspar precipitation and neomorphism have been observed in the Kawagarh Formation. ECC is characterized by subhedral to anhedral crystals that can also appear as fibrous crystals. Three types of ECC are identified in the Kawagarh Formation.

In the Kawagarh Formation, microspar is found in both interparticle and intraparticle pore spaces. It is present in the peripheral regions of skeletal particles such as planktonics, calcispheres, ostracods, pelecypods, inoceramids, echinoids, crinoids, trigonia, and textularia, as well as in the chambers of skeletal particles (Figure 3a,b). It becomes more prominent along the peripheries of skeletal particles in mudstones and wackstones (Figure 3c). In wackstones and packstones microfacies where grains are in contact, bladed crystals of Low Magnesium Calcite (LMC) cement envelope particles as isopachous cement (Figure 3e). The needle-like appearance of the LMC is due to the relict geometry of aragonite. In intraparticle pores, it occurs as the chamber fills in the form of interlocking mosaics (Figure 3b). Interlocking mosaics (sparite) are mainly comprised of anhedral to subhedral coarse crystals with fused edges. The interlocking crystals show extinction and exhibit light color.

4.1.2. Neomorphism

Neomorphism refers to transformations of mineral crystals caused by dissolution and reprecipitation in such a way that bulk chemistry remains intact [54,60,63]. Neomorphism includes the various types of transformations occurring in carbonate sediments like replacement, inversion, and recrystallization. Neomorphism is prominent in Kawagarh where the skeletal particles are recrystallized into coarse calcite crystals and micritic lime mud groundmass and already developed microspar affected by neomorphism and generally show the replacement of finer crystals with coarsely crystalline calcite. In marl or mudstone facies, the microspar tiny patches occur indicating neomorphism of micrite or lime mud (Figure 3f), and similarly skeletal particles show less effects of neomorphism. In wack-

stone and packstone microfacies, micrite and skeletal grains are significantly altered by neomorphism (Figures 3c,d and 4a,b). The skeletal particles of calcispheres and planktons are extensively replaced by coarse calcite (Figure 4a,b) in wackstone and packstone facies. Planktons (Figure 4b), trigonia, textularia (Figure 4f), echinoid (Figure 4c), and calcispheres (Figure 4a) are largely affected by neomorphism. However, filaments, oysters (Figure 4d), inoceramids (Figure 4f), and ostracods are less affected.

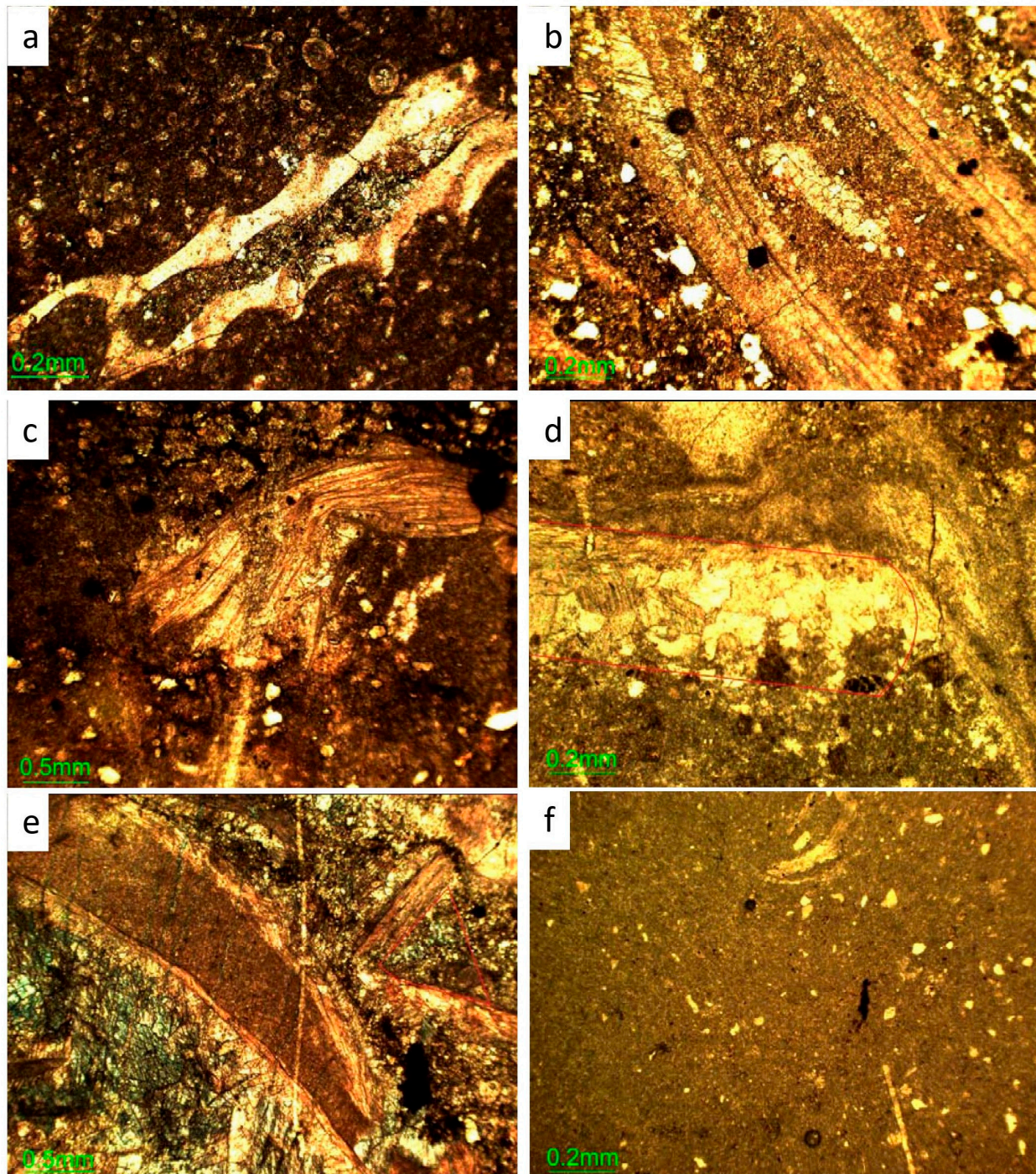


Figure 3. (a) Microspar filling in the bioclast, Sarbaroot Section. (b) Microspar filling in the oyster shell, Surg section. (c) Microspar along the lower periphery of oyster shell, Nawa section (d) Dripstone cement (indicated by red line) beneath the oyster shell, Jassian section. (e) Meniscus cement between the oyster shells (indicated by red line) and dripstone cement beneath the large oyster shell, Kalas Section. (f) Very minute effect of neomorphism.

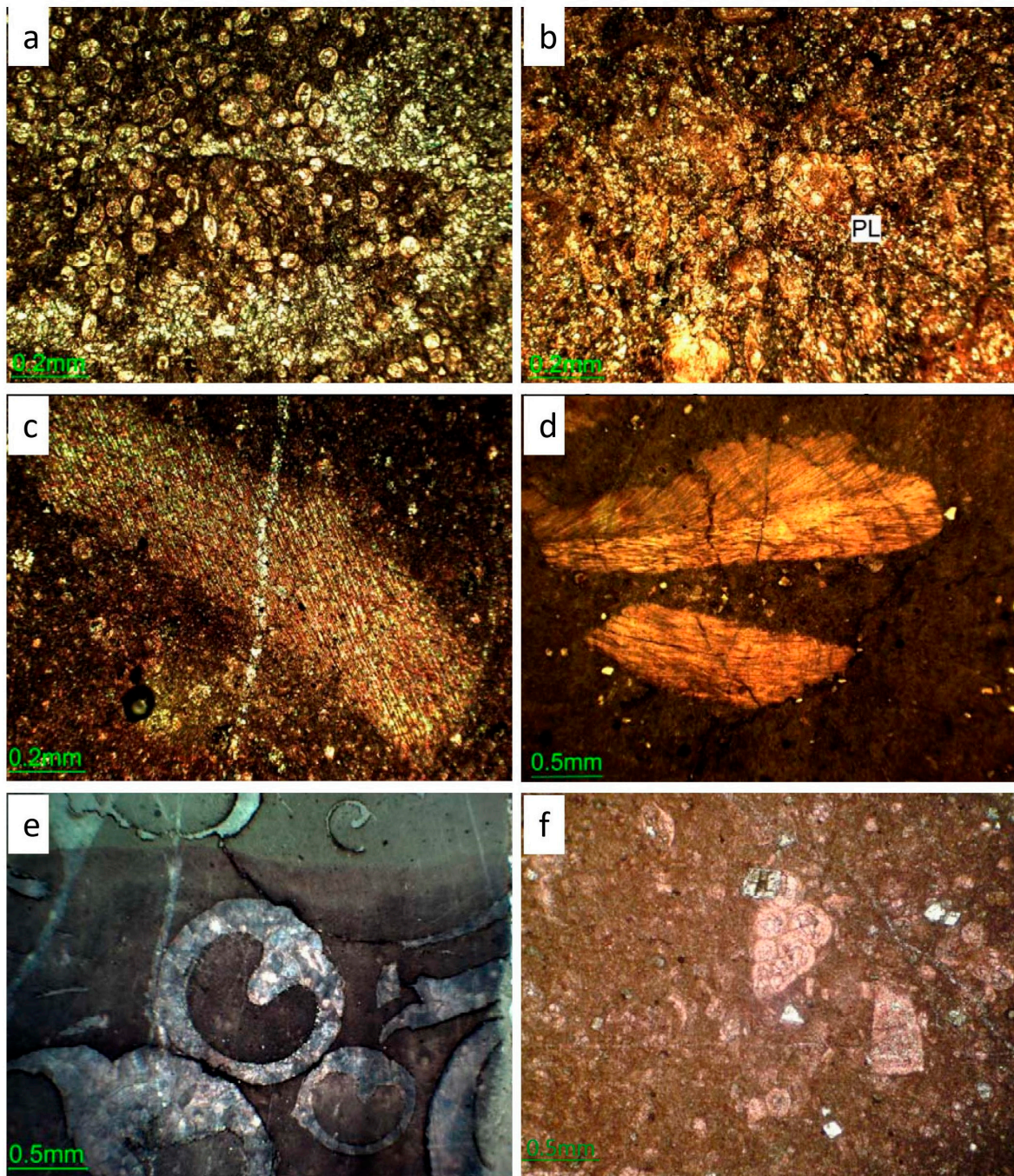


Figure 4. (a) Neomorphism in calcispheres packstone facies, Khanpur Section. (b) Neomorphism in plankton (PL) packstone facies, Bhag Neelab section. (c) Neomorphism in echinoid plate, Khanpur Section. (d) Unaltered oyster shells marking the absence of neomorphism in packstone, Akhori section. (e) Trigonias with neomorphosed periphery, Surg Section. (f) Textularias with neomorphosed chambers and blocky fragment of unaltered inoceramid, Thoba Section.

4.1.3. Compaction

Compaction is observed using common burial depth indicators such as orientation of burrows, particle interaction and deformation, porosity type, dissolution seams and their orientation, and overall texture of the rock.

- Mechanical Compaction

In carbonates, the mechanical compaction follows the distributed porosity and consequently from highly variable layer thickness with depth [64]. Since the recognition of mechanical compaction in fine-grained limestones is difficult, it is still evident largely in packstone microfacies (Figure 5a,b) by broken shells of skeletal particles, compressed particles, and close packing of skeletal particles. Two types of compactions are observed; the first type includes mechanical rearrangement of skeletal particles, which possibly occurred shortly after the aragonite dissolution or early calcite cementation; the second type of deformation brought ductile or brittle deformation in individual particles depending upon the particle mineralogy and shape. Breakage and deformation of skeletal particles are more distinct in plankton and pelecypods. Mechanical breakage is almost absent in calcispheres wherein instead these show close packing and concavo-convex contacts (Figure 4a). The breakage of skeletal particles in burrows is also extant (Figure 5a).

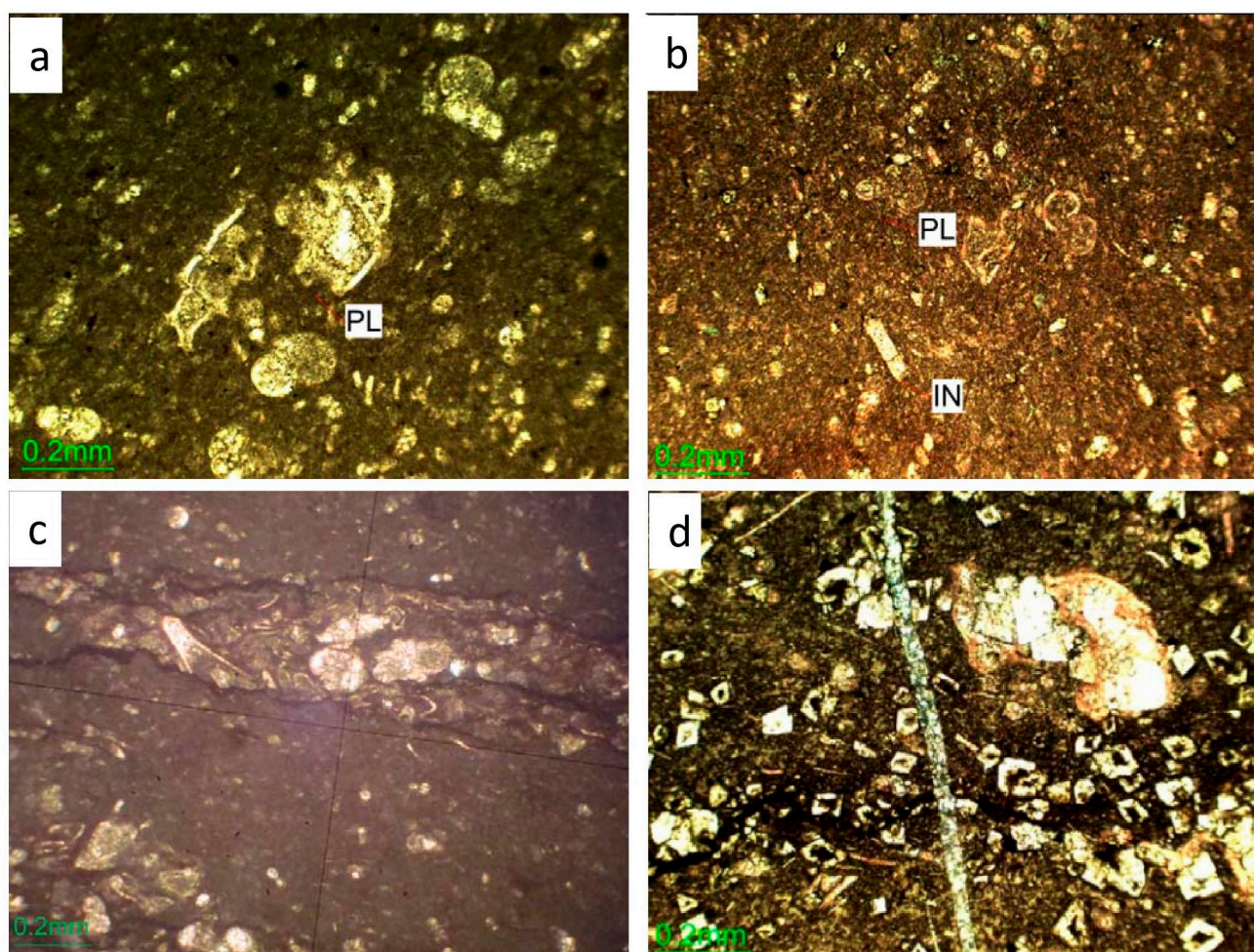


Figure 5. (a) Broken plankton (PL) in packstone, Kalas Section. (b) Broken and dissolved plankton (PL) and inoceramid (IN) in packstone, Chinali section. (c) Tightly packed broken plankton in burrow, Chinali Section. (d) Dolomitization along black stylolite structure, Thoba section.

- Chemical Compaction

Chemical compaction here mainly implies the removal of material via dissolution along pressure seams or stylolite, and subsequently transport of this material into the pores of the same system or elsewhere, causing overall compaction. Stylolites are irregular dissolution seams caused by the pressure solutions present in the intergranular space [65–67] which usually accommodate insoluble materials such as clay minerals, oxides, and organic matter transported by the pressure solution [68–70]. Initial chemical compaction starts with pressure solutioning of grains and grain contacts. Dissolved tests of skeletal particles have

also been recorded, sometimes with broken shells. (Figure 5a,b). These dissolved shells are dominantly planktonics showing sutured contacts (microstylolites) at places (Figure 5a,b).

- Stylolites

Outcrop studies revealed that stylolites define the sharp contacts and boundaries of dolomitized fronts and layers. In stratabound dolostone, stylolites are bedding-parallel, marking the contact between dolostones and limestones and frequently develop dolomitization fronts (Figure 6a). Stylolites show a variety of amplitudes with the highest at the Chinali outcrop associated with dolostones. In wackestone and packstone microfacies, stylolites exhibit abundant suture and sharp peak (Figure 6b) morphology, while mudstone facies dominate in wavy morphologies (Figure 6c).

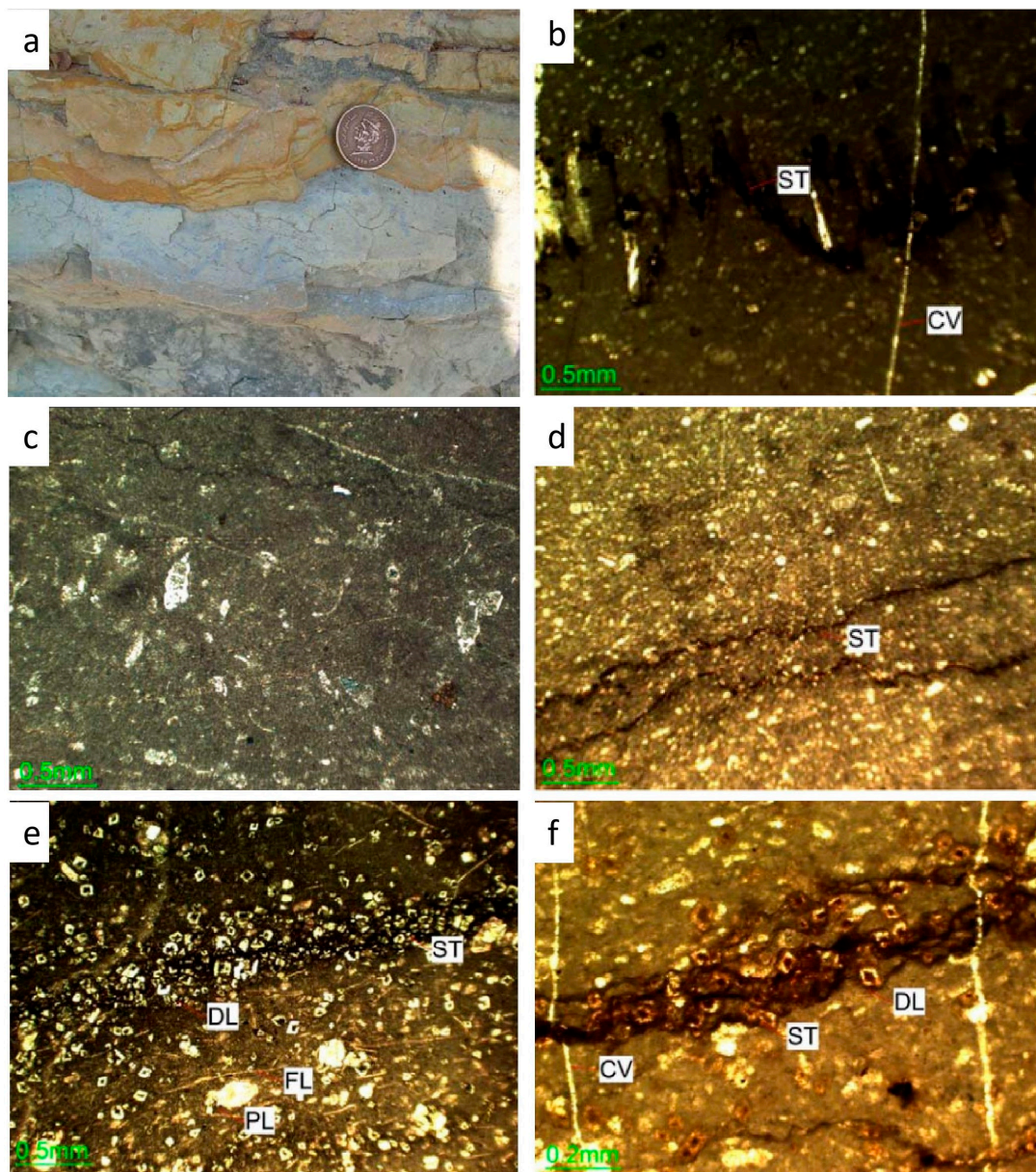


Figure 6. (a) Light grey limestone and yellowish-brown dolostone separated by stylolite (indicated by white arrows), Jassian section. (b) Sharpe peak stylolite, Chinali section. (c) Wavy stylolite in planktonic mudstone facies, Surg section. (d) Set of two wavy stylolites, Khanpur section. (e) Preferably developed rhombic dolomite (DL) crystals along black color stylolite (ST), Chinali section. (f) Rhombic dolomite (DL) with dark cores associated with yellowish and black colored stylolite (ST), calcite vein (CV) cutting through the stylolite.

In thin sections, the suture-and-sharp-peak (Figure 6b) and wave-like stylolites (Figure 6d), along with the associated reaction fronts, are not sharp but have a width of up to a few tens of microns. The single reaction front is bounded by a series of stylolites (Figures 6a and 7a,c). The seams of stylolites contain insoluble residues of iron oxide and clay material that can be recognized by the black and yellow colors, respectively (Figure 6e,f). In SEM, stylolites can easily be identified by the alignment of iron oxide between the rhombic dolomitic crystals (Figure 8a).

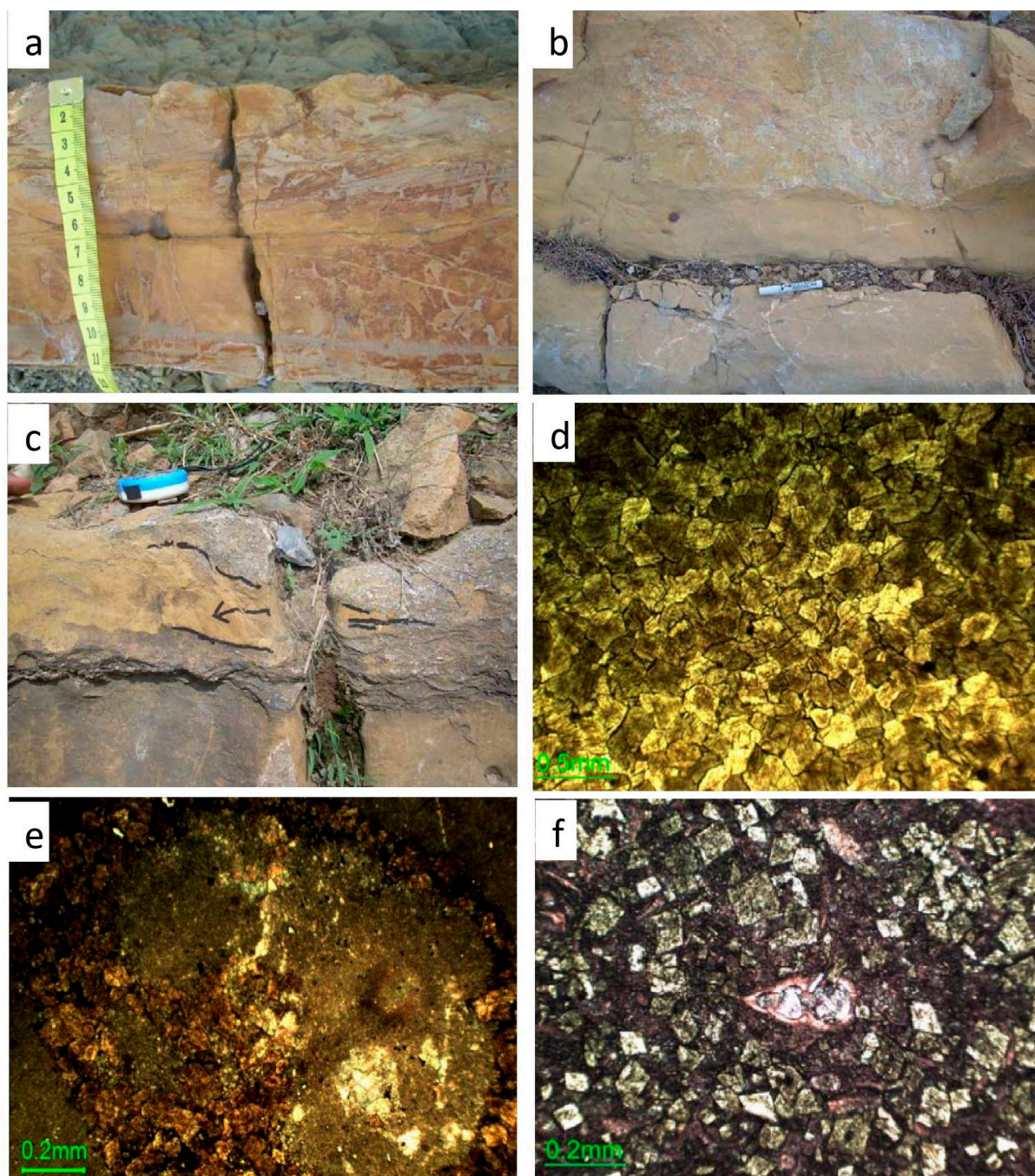


Figure 7. (a) Yellow to rusty brown, medium bedded dolostone, Jassian section. (b) Yellowish brown dolostone, Jassian section. (c) Dolomitization front (DF) and light yellow to yellowish grey dolomitized patches (DP) in limestone beds, Kalas section. (d) Mosaic of interlocking crystals of dolomite, Chinali Section. (e) Dolomitization along peripheries of trigonia indicated by arrow, Sarbaroot section. (f) Rhombic dolomite developed over the skeletal grain.

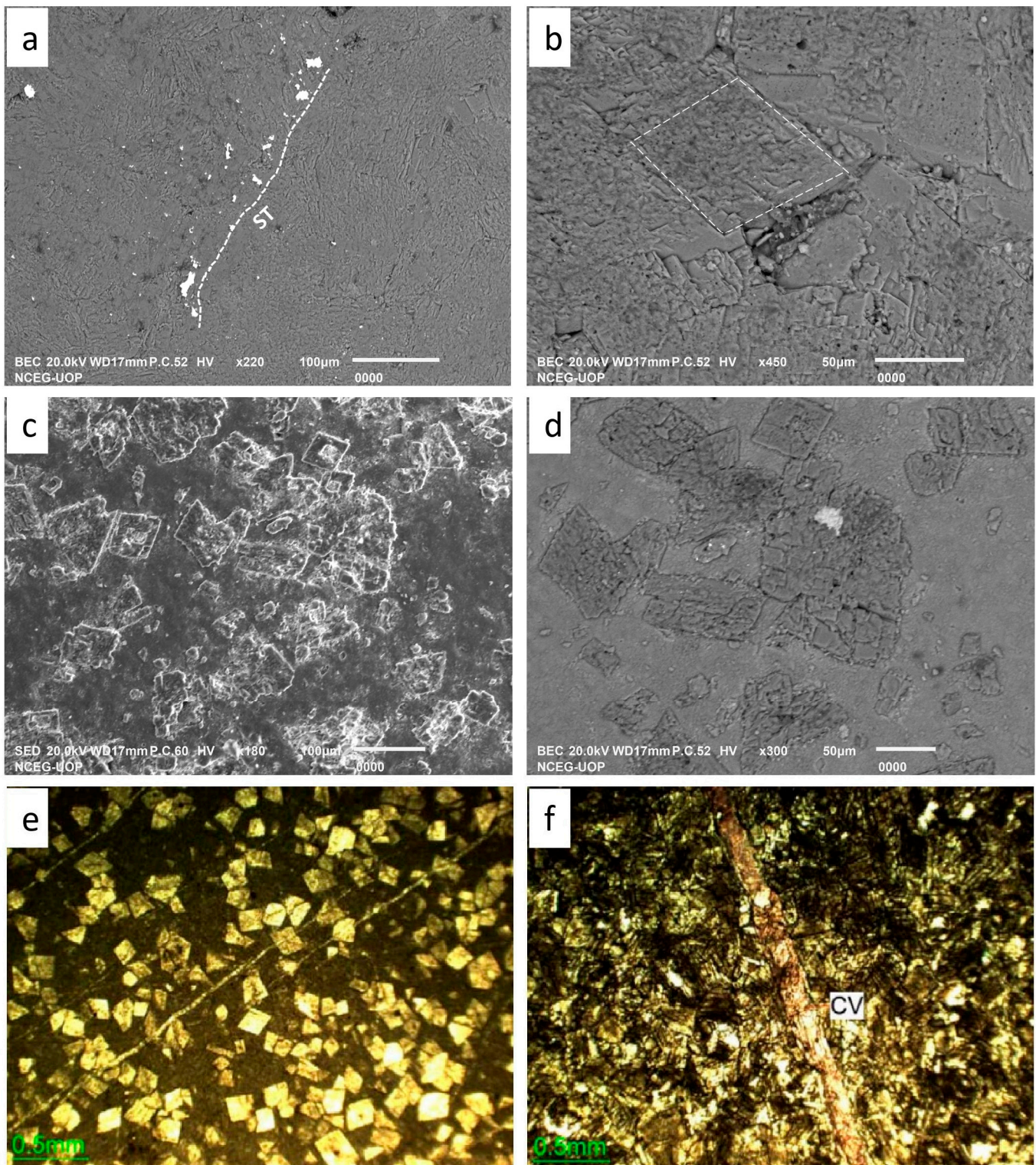


Figure 8. (a) BSE_SEM image showing stylolite identifiable by the alignment of iron oxide (white color), Chinali section. (b) A zoomed view “a” showing rhombic dolomite (DL). (c) SE_SEM image showing morphology of rhombic dolomite (DL) crystals, Jassian section. (d) BSE_SEM zoomed view of “b” showing rhombic polycrystalline dolomite (DL). (e) Individual rhombic dolomite crystals cross-cut by calcite veins. (f) Calcite vein cutting through mosaic dolomite whereby engulfed dolomite crystals in the vein are very clear.

4.1.4. Dolomitization

In the Kawagarh Formation, dolomites are found in two forms: 1—dolostone in stratabound dolomites (Figure 7a,b) and 2—dolomitic patches in partially dolomitized limestones (Figure 7c). The dolostone bodies are developed in the form of dolomite fronts bounded by bedding surfaces where whole beds are dolomitized. Dolomitic patches formed as a result of the partial dolomitization of limestone. Outcrop observations revealed that dolomitic patches regularly coincide with stylolites with sharp boundaries often bounded by stylolites (Figures 6a and 7c).

In the Hazara Basin, the maximum dolostone contents are observed at the Chinali section which accounts for 12% of the total samples, while the minimum dolostone contents (3% of the total samples) are recorded at the Sarbaroot section. In Kalachitta, dolostone is observed at the Surg and Jassian sections only, whereas the Akhori, Nawa, Sugdara, Bagh Neelab, and Sojhanda Bata sections show an absence of dolostone. Dolomitic patches appear in variable amounts at various levels of the Formation, however, dolostone bodies are confined to the lower part of the formation near the lower contact with the Lumshiwal Formation. Dolomitic limestone and dolostone are generally characterized by yellowish brown, rusty brown, and often light grey color with sandy texture.

Microscopic studies revealed that dolomite appears as individual rhombic crystals (Figures 6e,f and 8b–d) and mosaics of crystals (Figure 7d). Individual rhombic dolomite is referred to as replacive dolomite (RD1), while mosaic dolomite is referred to as replacive dolomite (RD2) here. RD1 appears in both dolomitic limestones and dolostones, while RD2 is exclusively present in dolostones. The dolomite crystals are generally characterized by the brown or yellowish-brown color (Figure 7d) in RD2, while yellowish brown to off-white with black spotted or rhombic cores in RD1 (Figures 5d and 7e,f). sRD1 are mostly euhedral (planar-p) dolomites with sharp edges, while RD2 are euhedral to subhedral (planar-s) dolomites (Figures 6f and 8b–d). The crystal size of RD1 is relatively finer ranging from 20 μm to 250 μm , while RD2 is coarser with crystal size ranging from 50 μm to 500 μm . RD2 extensively replaced skeletal and non-skeletal particles (Figure 7e,f), calcite, and micropor. The individual crystals of RD1 exhibit darker/black cores (Figures 5d and 7e,f). RD1 preferably populated along the stylolites (Figure 7e,f) where the dolomite crystals systematically superimpose over stylolites. Both destroy the fabric of the rock, however, RD1 exhibits intercrystallite porosity, while all the porosity is destroyed in RD2. RD1 and RD2 can easily be differentiated by distinct texture and color sometimes separated by stylolites.

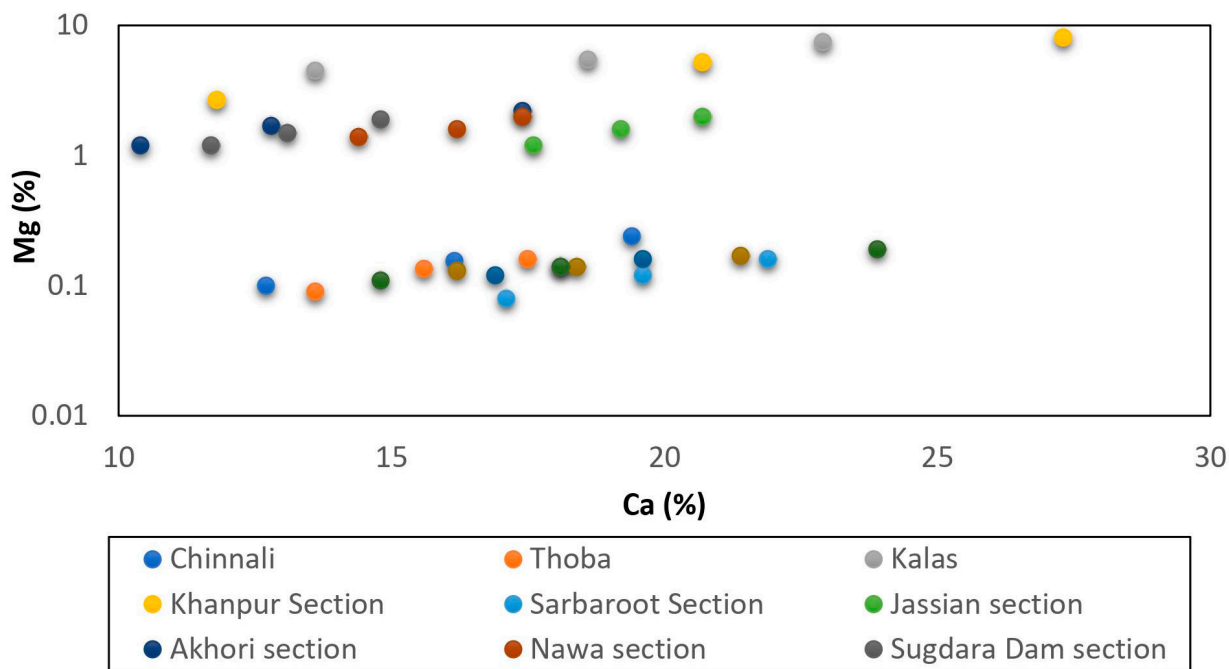
4.1.5. Calcite Veins and Fractures

Veins filled with bladed and/or coarse equant blocky calcite (FC) crystals occur as replacement and engulfment of components in the host limestones/dolostones. Euhedral dolomite crystals RD1 in the host dolostone that are engulfed by coarse-crystalline blocky calcite are unaltered or display evidence of partial to extensive calcitization (Figure 8e,f). Some of the coarse calcite crystals display undulous extinction and/or the presence of numerous sub-crystals. Calcite veins are the only features which crosscut the skeletal particles (Figure 4d), stylolites (Figure 6b,f), and dolomite crystals (Figure 8e). These veins show perpendicular to sub-perpendicular orientation to the bedding. Dedolomitization of dolomite and formation of calcite is obvious along these features (Figure 8f). These veins are thick where they cut skeletal particles and thin out in the distal areas.

4.2. Trace and Major Element Chemistry

The major elements, calcium and magnesium, show covariance across the sections, with mean values of 20.6% and 18.8%, respectively, with Ca ranging from 14.8% in Nawa to 23.9% in Sojhanda, and Mg ranging from 14.0% in Jassian to 23.6% in Bagh Neelab. The Khanpur, Sojhanda, and Bagh Neelab sections exhibit higher Mg content in the upper parts of Kawagarh, whereas in Jassian the Mg contents are high from the basal to the middle

parts, and in Kalas the basal and upper parts have higher Mg content. All other sections exhibit higher Mg occurrences only in the basal parts of Kawagarh (Figure 9).



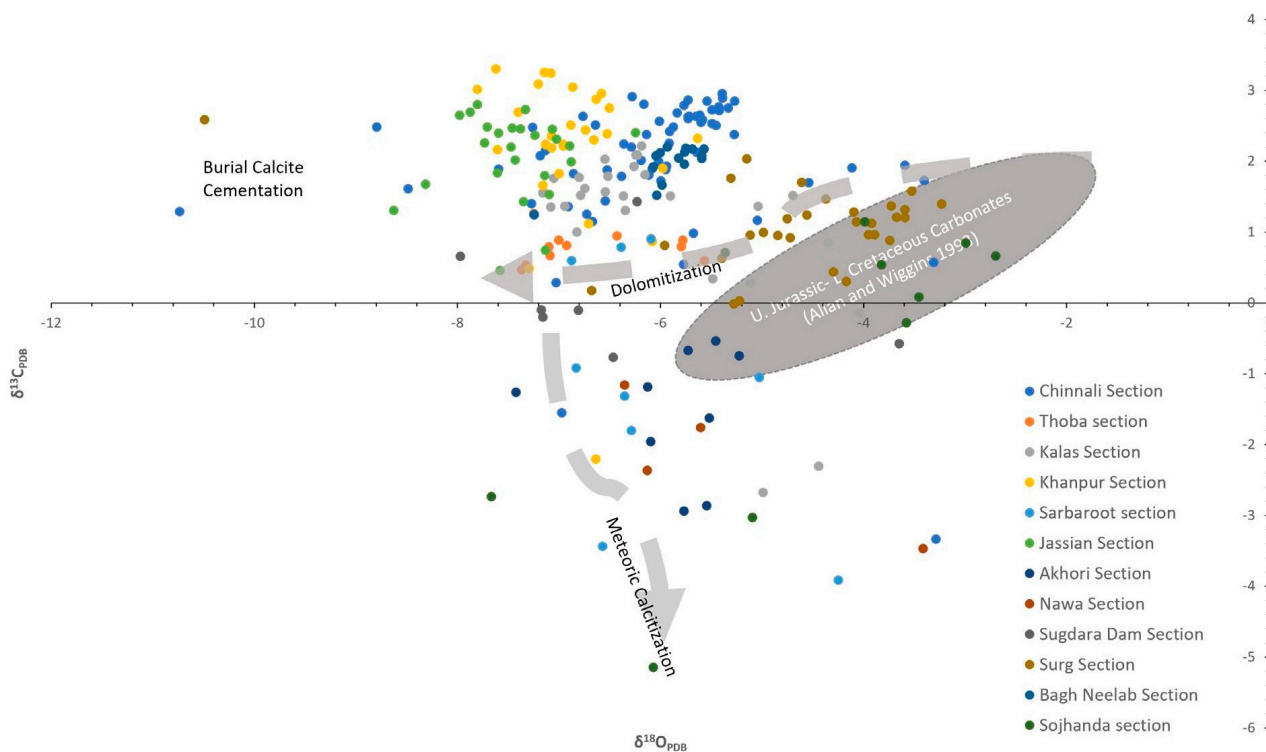


Figure 10. Carbon oxygen stable isotope cross plot showing the covariance in studied sections.

5. Discussion

5.1. Early Calcite Cementation

Microspar is a mosaic-like texture of inorganic calcite crystals ranging in grain size between 4 and 30 μm formed by secondary recrystallization of previously lithified micrite ($<4 \mu\text{m}$) after removal of Mg ions [71]. [72] discovered microspar cement in aragonite-dominated carbonate muds formed by meteoric diagenesis. The wider consensus has been established that microspar occurs from recrystallization of previously lithified micrite. However, there are examples [73,74] that chalks, although made of micrite, do not recrystallize to microspar even if subjected to fresh water meteoric diagenetic conditions. Many ancient carbonate systems do not experience meteoric conditions [75], which also raises the question about the origin of the microspar in them. [76] reported that microspar is recrystallized from lime mud as a primary cement in the early stages of marine burial diagenesis in Pliocene Bahamas carbonates and Silurian Gotland limestones. Despite the insufficient pressure and temperature condition, Munnecke suggested that strong geochemical gradients can be achieved by microbial decomposition of organic matter [77] in shallow burial environments which may dissolve and reprecipitate carbonates. According to [15,76,78], the pore fluid originated from the interlayer marls beds by the dissolution of aragonite, and then it was transported to the adjacent limestone bed where it was reprecipitated as LMC (microspar). Lately, a series of studies [78–81] led to a limestone–marl layer alternations model which is based on this diagenesis postulate that selective dissolution of aragonite in marl/limemud/shale beds and reprecipitation of calcite cement in limestone beds can result in a bed differentiation which can be confusing with the depositional cyclicality. The formation of microspar in the Kawagarh Formation is in accordance with the above model, evident by the alteration of marls with limestone, with no freshwater substantiations in the lower Kawagarh at early diagenetic stages. However, freshwater flux due to the subaerial exposure during the uplift events on the northern margin of the Indian plate is obvious owing to the India–Asia collision in the Upper Cretaceous (later stage of diagenesis). This cannot contribute to shallow burial early calcite cementation as the rock had already experienced the intermediate to deep burial.

The transformation of aragonite and high magnesium calcite (HMC) into microspar represents shallow marine burial diagenetic conditions. Furthermore, the isopachous cement is evidence of the marine Phreatic conditions.

5.2. Compaction

Mechanical compaction reflects in particle deformation, dewatering, and reduction in thickness and porosity [64,82–84]. Initially, mechanical compaction started with a few meters of burial depth characterized by dehydration and reduction in the thickness of sediment layers which led to close packing and a reduction in porosity. The dewatering of sediments resulted in plastic deformation which is characterized by the rearrangement of particles [85] and the deformation and breakage of skeletal particles [83]. Compaction-related porosity reduction is controlled by textures and dominant mineralogies. Other diagnostic features of mechanical compaction include deformed burrows, thinned and wispy laminations, broken and welded shells, broken micrite envelopes, and rotation and particle flattening [85–89]. In Kawagarh, mechanical compaction indicated by the skeletal particle rearrangement, breakage, deformation, and close contacts suggests burial depths of up to 100m. Mechanical compaction always shows greater signals in granular facies as the bigger grains take the first impact of the compaction, whereas the absence of preferred orientations and the neomorphism of intact grains supports how cementation took place before compaction [15]. Sutured skeletal particles contact and stylolite is clear evidence of pressure solutioning (chemical compaction) on depths >300 m and is indicative of the onset of burial diagenesis.

5.3. Dolomitization

Dolomitization refers to the replacement of limestone (CaCO_3) by dolomite ($\text{CaMg}(\text{CO}_3)_2$), which can occur in a variety of diagenetic settings. It is critical to establish key geochemical and environmental controls for various dolomitization models [3,90–92]. The fault-related hydrothermal dolomitization (HTD) model claims to explain the source of Mg by the convection of seawater along a rift-related open fault system and basal clastic aquifers [93–96]. Some studies also suggest thermodynamic ultramafic carbonation by the interaction of water and mafic/ultramafic rocks as the source of magnesium [97–99]. These views have modernized the thinking about the sources for water and magnesium in HTD. The same seems appropriate for the Late Cretaceous rifted northern margin of India [100] where the Kawagarh Formation deposited. A similar kind of diagenetic and dolomitization model has also been reported in Early Cretaceous Benicassim carbonates, Maestrat Basin, E. Spain [2,101,102]. Both the carbonates deposited in a rift basin share diagenetic similarities such as early calcite cementation, strata bound dolostones, stylolites, burial, and uplift. [6] has also reported similar Cambrian HTD dolomite bodies formed at shallow burial depths through hot brines, which were generated by high heat flows through faults in Cambrian rifting in dolomite from the Western Canadian Sedimentary Basin. These models justify the dolomitization in the Kawagarh Formation supported by stylolization paired with significant negative $\delta^{18}\text{O}$ values suggesting that the dolomitization occurred at intermediate to deep burial settings at higher temperatures negating the meteoric diagenesis. These HTD dolomite bodies often involve multiple stages of dolomitization [94,103,104] where a paragenetic sequence can be established by observing the cross-cutting relationship of different dolomite fabrics. In the Kawagarh Formation, the overlay of dolomitic crystals over stylolites suggests that stylolites were formed first and fed Mg for dolomitization. RD1 developed firstly and subsequently replaced by RD2 indicates multistage dolomitization [7]. In Figure 11, a schematic illustration shows how the evolving of dolomitization fronts can initiate RD1 and with time how RD1 can be replaced with RD2 euhedral and RD2 subhedral. Along the length of such fronts as it is recrystallizing the host, the depletion of Mg occurs ahead of the front levels only, forming individual crystals of RD1 with intercrystallite porosity.

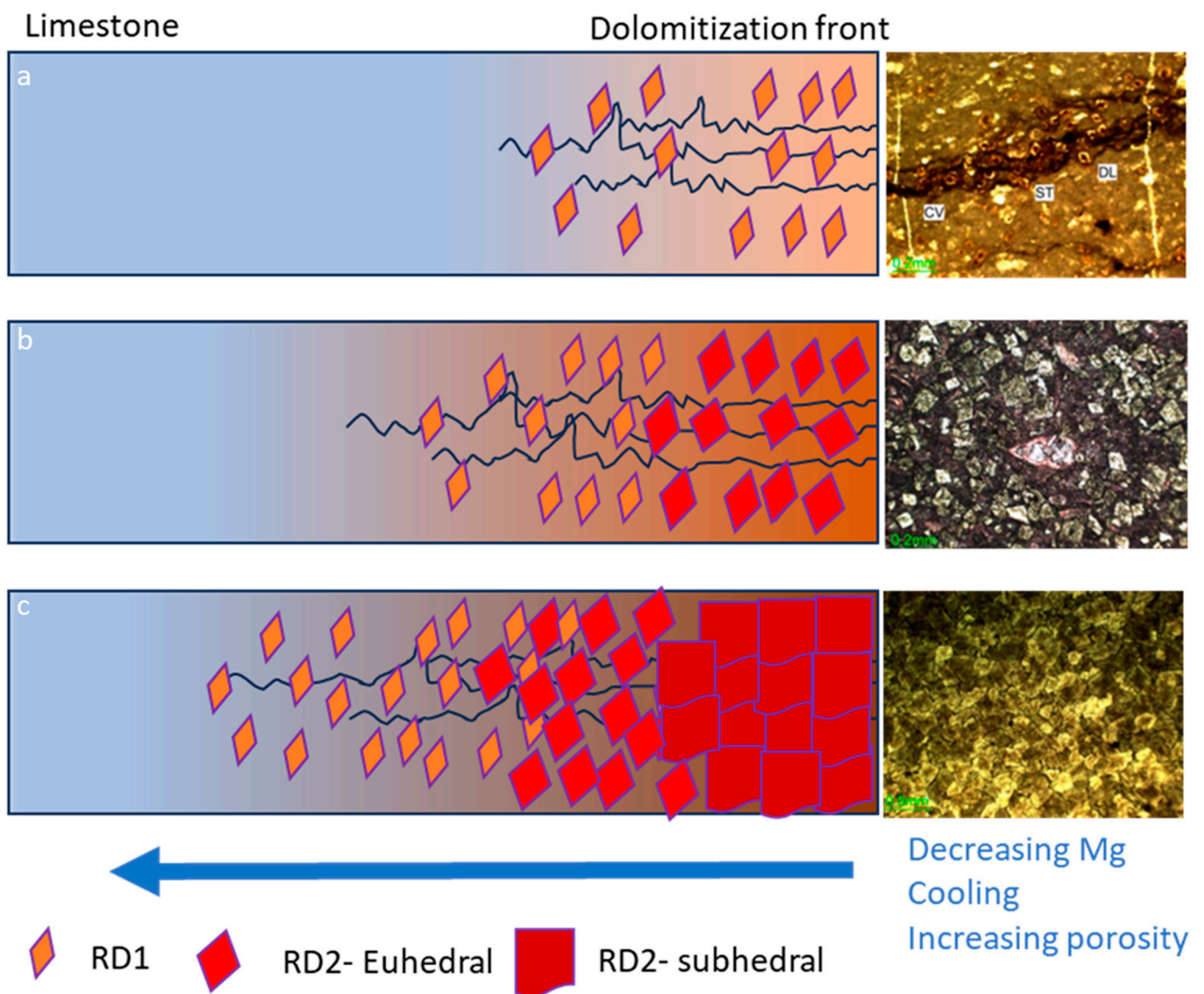


Figure 11. Systematic diagram showing evolution of the dolomitization front with time. (a) Initiation of the dolomitization front with RD1. (b) With the continued Mg influx and advancement of the front, this recrystallizes RD1 to euhedral RD2. (c) With further advancement, euhedral RD2 is recrystallized into subhedral RD2. Note how the fabric of the rock evolved along the length of the front with deleting and cooling fluid. Modified after [6].

5.4. Calcitisation

The ongoing India–Asia collision gradually uplifted the rock to shallower depths and produced fractures in lithified rock. Such shallow burial settings introduced low Mg undersaturated meteoric fluids which resulted in the transformation of dolomite to calcite through calcitisation. Depleted $\delta^{13}\text{C}$ values also suggest a likewise association (Figure 10). On the other hand, pronounced negative values of $\delta^{18}\text{O}$ negate the pure meteoric water influx and instead indicate the mixing of surface-derived waters with hot burial fluids. Frequent occurrence of FC with the dolomitisation fronts indicates that calcitising fluids flowed preferentially through the enhanced intercrystalline porosity of dolostones (Figure 8e,f). [6,7] reported similar calcitisation events where transformation from RD1 to calcite increased local porosity within dolostone. This suggests the process of calcitisation consists of two steps, an initial dissolution that enhances porosity around the periphery of dolostone bodies followed by a contemporaneous calcite cement (FC)

precipitation. The cross-cutting relationship and replacement of dolomite crystals along calcite fractures clearly indicates that these fractures postdate dolomitization.

5.5. Diagenetic Model

The Kawagarh Formation underwent four phases of diagenesis (Figure 12). In the first phase, early calcite cementation occurred during shallow marine burial, resulting in the formation of microspar cement by replacing micritic limemud matrix and bounding the skeletal grain. This also involves the dissolution of aragonite from limemud of marls into calcites of limestone. The later stage of the first phase corresponds to the neomorphism where the carbonate grain, particularly skeletal grains, were transformed into coarse-grained microspar calcite. The second phase corresponds to intermediate burial diagenesis, where mechanical and chemical compaction dominated with stylolization in the later stages. Stylolites formed at burial depths ranging between 300–800 m. Deep burial diagenesis corresponds to the third phase, which was characterized by dolomitization fronts, and the formation of RD1 and RD2 dolomite. The fourth and final phase corresponds to uplift, resulting in large-scale fractures and veins. Low Mg fresh fluids became incorporated into the system causing calcitisation (dedolomitization) and the precipitation of fracture calcite.

Phase		Shallow Burial	Intermediate Burial	Deep Burial	Uplift
Early Calcite Cementation (ECC)	Microspar	-----			
	Neomorphism		-----		
Compaction	Particle rearrangement and deformation		-----		
	Stylolites		-----		
Dolomitization	RD1			-----	
	RD2			-----	
Calcitization	FC				-----

Figure 12. Paragenetic history of the Kawagarh Formation showing the sequence of key diagenetic phases along with the time of formation.

6. Conclusions

The Kawagarh Formation was deposited during High Stand Tract (HST) under open shallow marine ramp environments, bounded by Low Stand (LST) clastics. The regional tectonic settings suggest that the depositional trend of the Kawagarh Formation was terminated by the initial collision of India with the KLA at the end of Cretaceous. The following conclusions can be drawn in context with the complex diagenetic history of the Kawagarh Formation by interpreting a multiproxy dataset integrating outcrop, petrographic, stable isotope, and geochemical data.

1. Early calcite cementation happened well before mechanical compaction which also inhibited later compaction in the Kawagarh Formation.
2. Predominantly, the dissolution of aragonite from lime mud in marls of the Kalachitta and high Mg calcite/aragonite from mudstones of the Hazara basin provided low Mg calcite for the precipitation of microspar.
3. The fault-related hydrothermal dolomitization model claims to explain the source of Mg by the convection of seawater along rift-related open fault systems and basal clastic aquifers for the Kawagarh formation.

4. The uplift related to the India–Asia collision introduced a fracture system and fresh low Mg fluid percolating the fracture system mixed with subsurface fluid caused the calcitisation in the Kawagarh Formation.

The present study provides significant insights about burial depths, fluid influx, the geochemical gradients, and the evolution of reservoir properties (porosity, permeability) of the formation as well as the basin itself, such as the depth and pressure at which it was buried, the fluid flow, and the geochemical gradients. This appraisal can be used to better understand the geologic history of the region and to develop better exploration strategies for hydrocarbon reservoirs.

Author Contributions: Conceptualization, S.U.R., N.A. and M.J.M.; methodology, S.U.R. and M.J.M.; software, M.J.M.; validation, M.M.S., N.A. and M.K.; formal analysis, M.J.M.; investigation, V.L. and G.K.; resources, S.U.R. and N.A.; data curation, M.J.M. and H.T.J.; writing—original draft preparation, S.U.R. and M.J.M.; writing—review and editing, N.A., M.M.S. and H.T.J.; visualization, M.J.M. and G.K.; supervision, N.A., M.M.S., V.L. and G.K.; project administration, S.U.R. All authors have read and agreed to the published version of the manuscript.

Funding: This research received no external funding.

Data Availability Statement: The data used in this work are available on request to the corresponding author(s).

Acknowledgments: This work benefited from numerous discussions and collaboration with Mohammad Al Suwaidi and Aleem Zahid. The first author would thank Meng Fanwei for technical support and experiments. The authors also acknowledge contributions from the University of Sargodha for field and logistics support.

Conflicts of Interest: The authors declare no conflict of interest.

References

1. Tomašových, A. Microfacies and depositional environment of an Upper Triassic intra-platform carbonate basin: The Fatric Unit of the West Carpathians (Slovakia). *Facies* **2004**, *50*, 77–105. [[CrossRef](#)]
2. Gomez-Rivas, E.; Martín-Martín, J.D.; Bons, P.D.; Koehn, D.; Griera, A.; Travé, A.; Llorens, M.-G.; Humphrey, E.; Neilson, J. Stylolites and stylolite networks as primary controls on the geometry and distribution of carbonate diagenetic alterations. *Mar. Pet. Geol.* **2022**, *136*, 105444. [[CrossRef](#)]
3. Whitaker, F.F.; Smart, P.L.; Jones, G.D. Dolomitization: From conceptual to numerical models. *Geom. Petrog. Dolomite Hydrocarb. Reserv.* **2004**, *235*, 99. [[CrossRef](#)]
4. Moore, C.H.; Wade, W.J. Carbonate Porosity and Introduction to Diagenesis. In *Carbonate Reservoirs*; Elsevier: Amsterdam, The Netherlands, 2013; p. 49.
5. Peyrotty, G.; Brigaud, B.; Martini, R. $\delta^{18}\text{O}$, $\delta^{13}\text{C}$, trace elements and REE in situ measurements coupled with U–Pb ages to reconstruct the diagenesis of upper triassic atoll-type carbonates from the Panthalassa Ocean. *Mar. Pet. Geol.* **2020**, *120*, 104520. [[CrossRef](#)]
6. Koeshidayatullah, A.; Corlett, H.; Stacey, J.; Swart, P.K.; Boyce, A.; Hollis, C. Origin and evolution of fault-controlled hydrothermal dolomitization fronts: A new insight. *Earth Planet Sci. Lett.* **2020**, *541*, 116291. [[CrossRef](#)]
7. Koeshidayatullah, A.; Corlett, H.; Stacey, J.; Swart, P.K.; Boyce, A.; Robertson, H.; Whitaker, F.; Hollis, C. Evaluating new fault-controlled hydrothermal dolomitization models: Insights from the Cambrian Dolomite, Western Canadian Sedimentary Basin. *Sedimentology* **2020**, *67*, 2945–2973. [[CrossRef](#)]
8. Alsuwaidi, M.; Mohamed, A.A.I.; Mansurbeg, H.; Morad, S.; Alsuwaidi, A.; Al-Shalabi, E.W.; Gomes, J.; Al-Ramadan, K.; Mohammed, I.Q.; Farouk, S. Depositional and diagenetic controls on reservoir quality of microporous basinal lime mudstones (Aptian), United Arab Emirates. *Sediment. Geol.* **2021**, *420*, 105925. [[CrossRef](#)]
9. Ehrenberg, S.N.; Nadeau, P.H. Sandstone vs. carbonate petroleum reservoirs: A global perspective on porosity-depth and porosity-permeability relationships. *Am. Assoc. Pet. Geol. Bull.* **2005**, *89*, 435–445. [[CrossRef](#)]
10. Morse, J.W.; Wade, W.J. Early Marine Diagenesis of Shal-Water Carbonate Sediments. In *Geochemistry of Sedimentary Carbonates*; Elsevier: Amsterdam, The Netherlands, 1990; pp. 241–276.
11. Tucker, M.E.; Bathurst, R.G. Carbonate diagenesis. In *International Association of Sedimentologists Series*, 1st ed.; Wiley–Blackwell: Hoboken, NJ, USA, 1990.
12. Moore, C.H.; Wade, W.J. Porosity Evolution in the Marine, Meteoric, and Burial Realms. In *Carbonate Reservoirs*; Elsevier: Amsterdam, The Netherlands, 2013; p. 91.
13. Regnet, J.B.; David, C.; Robion, P.; Menéndez, B. Microstructures and physical properties in carbonate rocks: A comprehensive review. *Mar. Pet. Geol.* **2019**, *103*, 366–376. [[CrossRef](#)]

14. Choquette, P.W.; Pray, L.C. Geologic Nomenclature and Classification of Porosity in Sedimentary Carbonates. *Am. Assoc. Pet. Geol. Bull.* **1970**, *54*, 207–250.
15. Munnecke, A.; Wright, V.P.; Nohl, T. The origins and transformation of carbonate mud during early marine burial diagenesis and the fate of aragonite: A stratigraphic sedimentological perspective. *Earth-Sci. Rev.* **2023**, *239*, 104366. [[CrossRef](#)]
16. Land, L.S. Limestone diagenesis—some geochemical considerations. *Geol. Surv. Bull.* **1986**, *5*, 129–137.
17. Choquette, P.W.; James, N.P. DIAGENESIS #12. Diagenesis in Limestones—3. The Deep Burial Environment. *Geosci. Can.* **1987**, *14*, 3–35.
18. Dutta, N.C. Deepwater geohazard prediction using prestack inversion of large offset P-wave data and rock model. *Lead. Edge* **2002**, *21*, 193–198. [[CrossRef](#)]
19. Ahsan, N. Facies Modeling, Depositional and Diagenetic Environments of Kawagarh Formation, Hazara Basin, Pakistan. Ph.D. Thesis, Punjab University, Lahore, Pakistan, 2008; Unpublished.
20. Rehman, S.; Ahsan, N.; Shah, M.; Munawar, M.; Miraj, M.; Rehman, F.; Mahmood, K. Depositional Environments and Microfacies of the Upper Turonian–Maastrichtian Kawagarh Formation, Kalachitta Range, Lesser Himalayas, Pakistan. *Aust. J. Earth Sci.* **2021**, *68*, 1017–1030. [[CrossRef](#)]
21. Latif, M. Explanatory Notes on the Geology of Southern Hazara to Accompany the Revised Geological Map. *Wein Jahrb Der Geol. Bundesanst.* **1970**, *15*, 5–20.
22. Calkins, J.A.; Offield, T.W.; Abdullah, S.K.M.; Ali, S.T. Geology of the southern Himalaya in Hazara, Pakistan and Adjoining Areas. Geol Surv Prof Pap 716-C, C1-C29 *Geol. Surv. Pakistan* **1975**, *19*, 93–132.
23. Aitchison, J.C.; Ali, J.R.; Davis, A.M. When and where did India and Asia collide? *J. Geophys. Res. Solid Earth* **2007**, *11*, 112–127. [[CrossRef](#)]
24. Ahsan, N.; Chaudhry, M.N. Geology of Hettangian to middle Eocene rocks of Hazara and Kashmir basins, Northwest lesser Himalayas, Pakistan. *Geol. Bull. Punjab Univ.* **2008**, *43*, 131–152.
25. Burg, J.-P.; Célérier, B.; Chaudhry, M.N.; Ghazanfar, M.; Gnehm, F.; Schnellmann, M. Fault analysis and paleostress evolution in large strain regions: Methodological and geological discussion of the southeastern Himalayan fold-and-thrust belt in Pakistan. *J. Asian Earth Sci.* **2005**, *24*, 445–467. [[CrossRef](#)]
26. Searle, M.P. Geological evidence against large-scale pre-Holocene offsets along the Karakoram Fault: Implications for the limited extrusion of the Tibetan Plateau. *Tectonics* **1996**, *15*, 171–186. [[CrossRef](#)]
27. Acton, G.D. Apparent polar wander of India since the Cretaceous with implications for regional tectonics and true polar wander, in the Indian Subcontinent and Gondwana: A Paleomagnetic and Rock Magnetic prospective. *Mem. Geol. Soc. India* **1999**, *44*, 129–175.
28. Ali, J.R.; Aitchison, J.C. Greater India. *Earth-Sci. Rev.* **2005**, *72*, 169–188. [[CrossRef](#)]
29. Najman, Y. The detrital record of orogenesis: A review of approaches and techniques used in the Himalayan sedimentary basins. *Earth-Sci. Rev.* **2006**, *74*, 1–72. [[CrossRef](#)]
30. Yin, A. Cenozoic tectonic evolution of the Himalayan orogen as constrained by along-strike variation of structural geometry, exhumation history, and foreland sedimentation. *Earth-Sci. Rev.* **2006**, *76*, 1–131. [[CrossRef](#)]
31. Gansser, A. *Geology of the Himalayas*; Interscience: New York, NY, USA, 1964; Volume 289.
32. Ghazanfar, M. Petrotectonic Elements and Tectonic Framework of Northwest Himalaya. Ph.D. Thesis, University of the Punjab, Punjab, Pakistan, 1993; Volume 1 & 2, pp. 1–380.
33. Powell, C.M. A speculative tectonic history of Pakistan and surroundings: Some constraints from the Indian Ocean. *Geodyn. Pak.* **1979**, *13*, 5–24.
34. Yeats, R.; Lawrence, R. Tectonics of the Himalayan thrust belt in northern Pakistan. In Proceedings of the US-Pakistan Workshop on Marine Sciences in Pakistan, Karachi, Pakistan, 11–16 November 1982; 39p.
35. Qureshi, K.A.; Ahmad, M. *Geological Map of Kalachitta Range, Northern Punjab, Pakistan*; Geological Survey of Pakistan: Quetta, Pakistan, 2001.
36. Latif, M.A.; Yasin, A.R.; Shafique, N.A.; Ashraf, M. Late mesozoic sedimentary megacycle in the rifted Haro Trough, Hazara, Pakistan and its hydrocarbon implications in the Northern Rim of the North West Himalayan Basin. *Pak. J. Hydrocarb. Res.* **1995**, *7*, 31–52.
37. Shah, S.M. *Stratigraphy of Pakistan*, 22nd ed.; Geological Survey of Pakistan: Quetta, Pakistan, 2009.
38. Rehman, S.U. Sedimentology of Turonian-Maastrichtian Kawagarh Formation, Attock Hazara Fold and Thrust Belt, Northwestern Lesser Himalayas, Pakistan. Doctoral Dissertation, University of Sargodha, Sargodha, Pakistan, 2017.
39. Garzanti, E.; Sciunnach, D.; Gaetani, M.; Corfield, R.; Watts, A.; Searle, M. Discussion on subsidence history of the north Indian continental margin, Zaskar–Ladakh Himalaya, NW India. *J. Geol. Soc. Lond.* **2005**, *162*, 889–892. [[CrossRef](#)]
40. Van Hinsbergen, D.J.; Lippert, P.C.; Dupont-Nivet, G.; McQuarrie, N.; Doubrovine, P.V.; Spakman, W.; Torsvik, T.H. Greater India Basin hypothesis and a two-stage Cenozoic collision between India and Asia. *Proc. Natl. Acad. Sci. USA* **2012**, *109*, 7659–7664. [[CrossRef](#)]
41. Rajkakati, M.; Bhowmik, S.K.; Ao, A.; Ireland, T.R.; Avila, J.; Clarke, G.L.; Aitchison, J.C. Thermal history of Early Jurassic eclogite facies metamorphism in the Nagaland Ophiolite Complex, NE India: New insights into pre-Cretaceous subduction channel tectonics within the Neo-Tethys. *Lithos* **2019**, *346*, 105166. [[CrossRef](#)]

42. Ahsan, N.; Rehman, S.U.; Shah, M.M. Kawagarh Formation (Turonian to Lower Maastrichtian)-A Homoclinal Ramp Deposit in Hazara Basin on Northern Margin of the Indian Plate. In Proceedings of the 15th Bathurst Meeting, Edinburgh, UK, 13–16 July 2015; University of Edinburgh: Edinburgh, UK, 2015.
43. Haq, B.U.; Hardenbol, J.; Vail, P.R. Mesozoic and Cenozoic chronostratigraphy and cycles of sea-level change. In *Society of Economic Paleontologists and Mineralogists*; Special Publication, 42; American Association of Petroleum Geoscience: Tulsa, OK, USA, 1988.
44. Rehman, S.U.; Mahmood, K.; Ahsan, N.; Shah, M. Microfacies and depositional environments of upper cretaceous Kawagarh Formation from Chinali and Thoba sections Northeastern Hazara Basin, lesser Himalayas, Pakistan. *J. Himal. Earth Sci.* **2016**, *49*, 1–16.
45. Chaudhry, M.N.; Mahmood, T.; Ahmed, R.; Ghazanfar, M. Microfacies, diagenesis and environment of deposition of Datta Formation from Jaster Gali, Abbottabad, Hazara, Pakistan. *Geol. Bull. Punjab Univ.* **1992**, *27*, 47–62.
46. Ding, L.; Kapp, P.; Wan, X. Paleocene–Eocene record of ophiolite obduction and initial India-Asia collision, south central Tibet. *Tectonics* **2005**, *24*, 1–18. [[CrossRef](#)]
47. Klootwijk, C.T.; Gee, J.; Peirce, J.; Smith, G. Constraints on the India-Asia convergence: Paleomagnetic results from Ninetyeast Ridge. In *Proceedings of the Ocean Drilling Program*; Scientific Results; Ocean Drilling Program: College Station, TX, USA, 1991; Volume 121.
48. Rehman, H.U.; Seno, T.; Yamamoto, H.; Khan, T. Timing of collision of the Kohistan–Ladakh Arc with India and Asia: Debate. *Isl. Arc* **2011**, *20*, 308–328. [[CrossRef](#)]
49. Spencer, D.A. *Tectonics of the Higher-and Tethyan Himalaya, Upper Kaghan Valley, NW Himalaya, Pakistan: Implications of an Early Collisional, High Pressure (Eclogite Facies) Metamorphism to the Himalayan Belt*; Eidgenössische Technische Hochschule Zuerich: Zürich, Switzerland, 1993.
50. Yin, A.; Harrison, T.M. Geologic evolution of the Himalayan-Tibetan orogen. *Annu. Rev. Earth Planet. Sci.* **2000**, *28*, 211–280. [[CrossRef](#)]
51. Dickson, J.A.D. A Modified Staining Technique for Carbonates in Thin Section. *Nature* **1965**, *205*, 587. [[CrossRef](#)]
52. Adams, A.; MacKenzie, I. *Carbonate Sediments and Rocks under the Microscope: A Colour Atlas*, 1st ed.; CRC Press: Boca Raton, FL, USA, 1998.
53. Robinson, P. Determination of calcium, magnesium, manganese, strontium, sodium and iron in the carbonate fraction of limestones and dolomites. *Chem. Geol.* **1980**, *28*, 135–146. [[CrossRef](#)]
54. Folk, R.L. Some Aspects of Recrystallization in Ancient Limestones¹. In *Dolomitization and Limestone Diagenesis*; SEPM Society for Sedimentary Geology: Tulsa, OK, USA, 1965; Volume 13.
55. Bathurst, R. Chapter 12 Neomorphic Processes in Diagenesis. In *Carbonate Sediments and Their Diagenesis; Developments in Sedimentology*; Elsevier: Amsterdam, The Netherlands, 1972; pp. 475–516.
56. James, N.P.; Choquette, P.W. Diagenesis 5. Limestones: Introduction. *Geosci. Can.* **1983**, *10*. Available online: <https://journals.lib.unb.ca/index.php/GC/article/view/3352> (accessed on 1 November 2023).
57. Tucker, M.E.; Wright, V.P. Diagenetic Processes, Products and Environments. *Carbonate Sedimentol.* **1990**, *314*, 364.
58. Neumeier, U. Experimental modelling of beachrock cementation under microbial influence. *Sediment. Geol.* **1999**, *126*, 35–46. [[CrossRef](#)]
59. Hillgärtner, H.; Dupraz, C.; Hug, W. Microbially induced cementation of carbonate sands: Are micritic meniscus cements good indicators of vadose diagenesis? *Sedimentology* **2001**, *48*, 117–131. [[CrossRef](#)]
60. Flügel, E. (Ed.) *Diagenesis, Porosity, and Dolomitization BT—Microfacies of Carbonate Rocks: Analysis, Interpretation and Application*; Springer: Berlin/Heidelberg, Germany, 2004; pp. 267–338.
61. Boggs, S. *Principles of Sedimentology and Stratigraphy*; Pearson Prentice Hall: Hoboken, NJ, USA, 2006.
62. Reinhold, C.; Kaufmann, B. Sea-level changes as controlling factor of early diagenesis: The reefal limestones of Adnet (Late Triassic, Northern Calcareous Alps, Austria). *Facies* **2010**, *56*, 231–248. [[CrossRef](#)]
63. Flügel, E. (Ed.) *Karbonatdiagenese BT—Mikrofazielle Untersuchungsmethoden von Kalken*; Springer: Berlin/Heidelberg, Germany, 1978; pp. 51–78.
64. Smith, J.E. The dynamics of shale compaction and evolution of pore-fluid pressures. *J. Int. Assoc. Math. Geol.* **1971**, *3*, 239–263. [[CrossRef](#)]
65. Koehn, D.; Renard, F.; Toussaint, R.; Passchier, C.W. Growth of stylolite teeth patterns depending on normal stress and finite compaction. *Earth Planet Sci. Lett.* **2007**, *257*, 582–595. [[CrossRef](#)]
66. Ebner, M.; Piazzolo, S.; Renard, F.; Koehn, D. Stylolite interfaces and surrounding matrix material: Nature and role of heterogeneities in roughness and microstructural development. *J. Struct. Geol.* **2010**, *32*, 1070–1084. [[CrossRef](#)]
67. Toussaint, R.; Aharonov, E.; Koehn, D.; Gratier, J.P.; Ebner, M.; Baud, P.; Rolland, A.; Renard, F. Stylolites: A review. *J. Struct. Geol.* **2018**, *114*, 163–195. [[CrossRef](#)]
68. Nelson, R.A. Significance of fracture sets associated with stylolite zones: Geologic notes. *Am. Assoc. Pet. Geol. Bull.* **1981**, *65*, 2417–2425.
69. Railsback, L.B. Lithologic controls on morphology of pressure-dissolution surfaces (stylolites and dissolution seams) in Paleozoic carbonate rocks from the mideastern United States. *J. Sediment. Res.* **1993**, *63*, 513–522. [[CrossRef](#)]

70. Ben-Itzhak, L.L.; Aharonov, E.; Karcz, Z.; Kaduri, M.; Toussaint, R. Sedimentary stylolite networks and connectivity in limestone: Large-scale field observations and implications for structure evolution. *J. Struct. Geol.* **2014**, *63*, 106–123. [[CrossRef](#)]
71. Folk, R.L. Practical Petrographic Classification of Limestones. *Am. Assoc. Pet. Geol. Bull.* **1995**, *43*, 1–38. [[CrossRef](#)]
72. Lasemi, Z.; Sandberg, P.A. Transformation of aragonite-dominated lime muds to microcrystalline limestones. *Geology* **1984**, *12*, 420–423. [[CrossRef](#)]
73. Beales, F.W. Conditions of Deposition of Palliser (Devonian) Limestone of Southwestern Alberta. *Am. Assoc. Pet. Geol. Bull.* **1956**, *40*, 848–870. [[CrossRef](#)]
74. James, N.P.; Choquette, P.W. Diagenesis 9. Limestones—The Meteoric Diagenetic Environment. *Geosci. Can.* **1984**, *11*, 161–194.
75. Bathurst, R.G.C. Microfabrics in Carbonate Diagenesis: A Critical Look at Forty Years in Research. In *Carbonate Microfabrics*; Rezak, R., Lavoie, D.L., Eds.; Springer: New York, NY, USA, 1993; pp. 3–14.
76. Munnecke, A.; Westphal, H.; Reijmer, J.; Samtleben, C. Microspar development during early marine burial diagenesis: A comparison of Pliocene carbonates from the Bahamas with Silurian limestones from Gotland (Sweden). *Sedimentology* **1997**, *44*, 977–990. [[CrossRef](#)]
77. Canfield, D.E.; Raiswell, R. Carbonate Precipitation and Dissolution: Its Relevance to Fossil Preservation. *Geography* **1991**, 411–453. Available online: <https://www.semanticscholar.org/paper/Carbonate-Precipitation-and-Dissolution%3A-Its-to-Canfield-Raiswell/3bc334ef1bc6aa986a81739738ddcb5071324a9b> (accessed on 1 November 2023).
78. Munnecke, A.; Westphal, H. Variations in primary aragonite, calcite, and clay in fine-grained calcareous rhythmites of Cambrian to Jurassic age—An environmental archive? *Facies* **2005**, *51*, 592–607. [[CrossRef](#)]
79. Munnecke, A.; Westphal, H.; Elrick, M.; Reijmer, J. The mineralogical composition of precursor sediments of calcareous rhythmites: A new approach. *Int. J. Earth Sci.* **2001**, *90*, 795–812. [[CrossRef](#)]
80. Westphal, H.; Böhm, F.; Bornholdt, S. Orbital frequencies in the carbonate sedimentary record: Distorted by diagenesis? *Facies* **2004**, *50*, 3–11. [[CrossRef](#)]
81. Westphal, H.; Munnecke, A.; Böhm, F.; Bornholdt, S. Limestone-marl alternations in epeiric sea settings—Witnesses of environmental changes, or of rhythmic diagenesis? *Geol. Assoc. Can.* **2008**, *48*, 389–406.
82. Shinn, E.A.; Halley, R.B.; Hudson, J.H.; Lidz, B.H. Limestone compaction: An enigma. *Geology* **1977**, *5*, 21–24. [[CrossRef](#)]
83. Shinn, E.A.; Robbin, D.M. Mechanical and chemical compaction in fine-grained shallow-water limestones. *J. Sediment. Res.* **1983**, *53*, 595–618. [[CrossRef](#)]
84. Gnoli, M. The amount of the taphonomic/tectonic compaction in the Fluminimaggiore Formation (SW Sardinia, Italy) with discussion of a new paleontological method for estimating compaction. *Palaeontol. Electron.* **2002**, *4*, 18–37.
85. Ricken, W. *Diagenetic Bedding: A Model for Marl-Limestone Alternations (Lecture Notes in Earth Sciences #6)*; Springer: New York, NY, USA, 1986.
86. Bathurst, R. The integration of pressure solution with mechanical compaction and cementation. In *Stylolites and Associated Phenomena. Relevance to Hydrocarbon Reservoirs*; Abu Dhabi Natl Reserv Found: Abu Dhabi, United Arab Emirates, 1984; pp. 41–55.
87. Lasemi, Z.; Sandberg, P.A.; Boardman, M.R. New microtextural criterion for differentiation of compaction and early cementation in fine-grained limestones. *Geology* **1990**, *18*, 370–373. [[CrossRef](#)]
88. Monaco, C.; Tortorici, L.; Nicolich, R.; Cernobori, L.; Costa, M. From collisional to rifted basins: An example from the southern Calabrian arc (Italy). *Tectonophysics* **1996**, *266*, 233–249. [[CrossRef](#)]
89. Westphal, H.; Munnecke, A. Mechanical compaction versus early cementation in fine-grained limestones: Differentiation by the preservation of organic microfossils. *Sediment. Geol.* **1997**, *112*, 33–42. [[CrossRef](#)]
90. Morrow, D.W. Diagenesis 2. Dolomite—Part 2 Dolomitization Models and Ancient Dolostones. *Geosci. Can.* **1982**, *9*, 95–107.
91. Land, L.S. The Origin of Massive Dolomite. *J. Geol. Educ.* **1985**, *33*, 112–125. [[CrossRef](#)]
92. Machel, H.G. Concepts and models of dolomitization: A critical reappraisal. *Geom. Petrog. Dolomite Hydrocarb. Reserv.* **2004**, *235*, 7–63. [[CrossRef](#)]
93. Martín-Martín, J.; Travé, A.; Gomez-Rivas, E.; Salas, R.; Sizun, J.-P.; Vergés, J.; Corbella, M.; Stafford, S.; Alfonso, P. Fault-controlled and stratabound dolostones in the Late Aptian–earliest Albian Benassal Formation (Maestrat Basin, E Spain): Petrology and geochemistry constrains. *Mar. Pet. Geol.* **2015**, *65*, 83–102. [[CrossRef](#)]
94. Hollis, C.; Bastesen, E.; Boyce, A.; Corlett, H.; Gawthorpe, R.; Hirani, J.; Rotevatn, A.; Whitaker, F. Fault-controlled dolomitization in a rift basin. *Geology* **2017**, *45*, 219–222. [[CrossRef](#)]
95. Hirani, J.; Bastesen, E.; Boyce, A.; Corlett, H.; Eker, A.; Gawthorpe, R.; Hollis, C.; Korneva, I.; Rotevatn, A. Structural controls on non-fabric-selective dolomitization within rift-related basin-bounding normal fault systems: Insights from the Hammam Faraun Fault, Gulf of Suez, Egypt. *Basin Res.* **2018**, *30*, 990–1014. [[CrossRef](#)]
96. Al-Ramadan, K.; Koeshidayatullah, A.; Cantrell, D.; Swart, P.K. Impact of basin architecture on diagenesis and dolomitization in a fault-bounded carbonate platform: Outcrop analogue of a pre-salt carbonate reservoir, Red Sea rift, NW Saudi Arabia. *Pet. Geosci.* **2019**, *26*, 448–461. [[CrossRef](#)]
97. Lavoie, D.; Jackson, S.; Girard, I. Magnesium isotopes in high-temperature saddle dolomite cements in the lower Paleozoic of Canada. *Sediment. Geol.* **2014**, *305*, 58–68. [[CrossRef](#)]
98. Falk, E.S.; Kelemen, P.B. Geochemistry and petrology of listvenite in the Samail ophiolite, Sultanate of Oman: Complete carbonation of peridotite during ophiolite emplacement. *Geochim. Cosmochim. Acta* **2015**, *160*, 70–90. [[CrossRef](#)]

99. Robertson, H.; Corlett, H.; Hollis, C.; Kibblewhite, T.; Whitaker, F. Listwanitization as a Source of Mg for Dolomitization: Field Evaluation in Atlin, British Columbia. In Proceedings of the Goldschmidt Conference, Barcelona, Spain, 18–23 August 2019.
100. Garzanti, E.; Hu, X. Latest Cretaceous Himalayan tectonics: Obduction, collision or Deccan-related uplift? *Gondwana Res.* **2015**, *28*, 165–178. [[CrossRef](#)]
101. Humphrey, E.; Gomez-Rivas, E.; Neilson, J.; Martín-Martín, J.D.; Healy, D.; Yao, S.; Bons, P.D. Quantitative analysis of stylolite networks in different platform carbonate facies. *Mar. Pet. Geol.* **2020**, *114*, 104203. [[CrossRef](#)]
102. Yao, S.; Gomez-Rivas, E.; Martín-Martín, J.D.; Gómez-Gras, D.; Travé, A.; Griera, A.; Howell, J. A Fault-controlled dolostone geometries in a transgressive–regressive sequence stratigraphic framework. *Sedimentology* **2020**, *67*, 3290–3316. [[CrossRef](#)]
103. Davies, G.R.; Smith, L.B., Jr. Structurally controlled hydrothermal dolomite reservoir facies: An overview. *Am. Assoc. Pet. Geol. Bull.* **2006**, *90*, 1641–1690. [[CrossRef](#)]
104. Sharp, I.; Gillespie, P.; Morsalnezhad, D.; Taberner, C.; Karpuz, R.; Vergés, J.; Horbury, A.; Pickard, N.; Garland, J.; Hunt, D. Stratigraphic architecture and fracture-controlled dolomitization of the Cretaceous Khami and Bangestan groups: An outcrop case study, Zagros Mountains, Iran. In *Mesozoic and Cenozoic Carbonate Systems of the Mediterranean and the Middle East: Stratigraphic and Diagenetic Reference Models*; Geological Society: London, UK, 2010; Volume 329, pp. 343–396.

Disclaimer/Publisher’s Note: The statements, opinions and data contained in all publications are solely those of the individual author(s) and contributor(s) and not of MDPI and/or the editor(s). MDPI and/or the editor(s) disclaim responsibility for any injury to people or property resulting from any ideas, methods, instructions or products referred to in the content.